A Thermodynamic Equilibrium Climate Model for Monthly Mean Surface Winds and Precipitation over the Tropical Pacific

TIANMING LI AND BIN WANG

Department of Meteorology, School of Ocean and Earth Science and Technology, University of Hawaii at Manoa, Honolulu, Hawaii

(Manuscript received 5 October 1992, in final form 17 May 1993)

ABSTRACT

Diagnosis of the dynamic and thermodynamic balances using observed climatological monthly mean data reveals that 1) anisotropic, latitude-dependent Rayleigh friction coefficients lead to much improved modeling of the monthly mean surface wind field for a given monthly mean sea level pressure field, and 2) the annual variation of the vertically averaged lapse rate is important for modeling sea level pressure.

Based on the aforementioned observations, a thermodynamic equilibrium climate model for the tropical Pacific is proposed. In this model, the sea level pressure is thermodynamically determined from sea surface temperature (SST) through a vertically integrated hydrostatic equation in which the vertical mean lapse rate is a function of SST plus a time-independent correction. The surface winds are then computed from sea level pressure gradients through a linear surface momentum balance with anisotropic, latitude-dependent Rayleigh friction coefficients. The precipitation is finally obtained from a moisture budget by taking into account the effects of SST on convective instability.

Despite its simplicity, the model is capable of simulating realistic annual cycles as well as interannual variations of the surface wind, sea level pressure, and precipitation over the tropical Pacific. The success of the model suggests that the tropical atmosphere on a monthly mean time scale is, to the lowest-order approximation, in a thermodynamic equilibrium state in which sea level pressure is primarily controlled by SST and the effects of dynamic feedback on sea level pressure may be parameterized by an empirical SST–lapse rate relationship. Further studies are needed to establish a firm physical basis for the proposed parameterization.

1. Introduction

A large number of simple or intermediate coupled ocean–atmosphere models have been developed in the past decade for study of the variability of the tropical atmosphere and ocean. A key element for the atmospheric component is prediction of surface winds and precipitation/cloudiness for a given sea surface temperature (SST) forcing.

Gill's (1980) single vertical mode model for studying atmospheric response to imposed heating has been the basic dynamic framework for most simple atmospheric models. Zebiak (1982) assumed evaporational heating proportional to SST and its anomaly, and later (Zebiak 1986) included a circulation-dependent moisture convergence feedback following Webster (1981). Davey and Gill (1987) considered the Newtonian cooling process as thermal forcing through which the atmosphere tends to relax toward an equilibrium state controlled by SST. Seager (1991) considered the importance of buoyancy in representation of convective heating.

Wang and Li (1993, WL hereafter) proposed a nonlinear SST-dependent atmospheric heating scheme in which the atmospheric heating essentially incorporates all three thermodynamic processes described in the aforementioned models. In addition, SST gradient effects on boundary-layer momentum balance (Lindzen and Nigam 1987) were also included and the importance of the interaction between boundary-layer and free atmosphere flows was emphasized. The model can reproduce both a shallow intertropical convergence zone in the boundary layer and a deep South Pacific convergence zone and monsoon troughs in the lower troposphere.

In spite of the forgoing successes, the physics included in these simple or intermediate models are limited and insufficient for simulating an accurate monthly mean sea level pressure or surface wind field. One of the purposes of this study is to analyze detailed dynamic and thermodynamic balances using observed climatological monthly mean data and to understand the way these models work and their inherent limitations.

For the purpose of coupled atmosphere–ocean modeling, the most important requirement for an atmosphere model is to produce accurate wind fields for given SST forcing. Monthly mean surface winds can be determined from the surface pressure field, provided the frictional and transient eddy effects can be param-

Corresponding author address: Dr. Bin Wang, University of Hawaii at Manoa, Department of Meteorology, 2525 Correa Road, Honolulu, HI 96822.

eterized by a large-scale wind field. How important is the nonlinearity of transient disturbances to time-mean momentum balance? How do we adequately parameterize these transient effects if they are important? These issues need to be addressed. Because the Coriolis force vanishes at the equator, a moderate pressure gradient can generate surface winds of considerable magnitude. A fundamental difficulty in reproducing accurate surface winds lies in the simulation of a sufficiently accurate surface pressure field.

Observation shows a high correlation between climatological monthly mean SST and sea level pressure (SLP). Inspection of the tropical marine climatic atlas by Sadler et al. (1987) discloses an obvious linkage between SLP and SST. In the western Pacific the highest SST is located at 10°S in January and moves to 15°N in July. The sea surface pressure shows a similar shift with minimum pressure at 10°S (northwest of Australia) in January and 10°–20°N (northwestern Pacific) in July. The cold SST tongues in the eastern North and South Pacific are located east of the subtropical high systems in the Northern and Southern Hemispheres, respectively. The near-equatorial trough is strongest in July along 10°N and weakest in January along 5°N, closely following the annual shift of the warm water zone as indicated by the 27.5°C SST contour along 8°–10°N in July and a contour line of 26.5°C along 5°–8°N in January.

Motivated by the forgoing observations, we attempted to develop a highly parameterized thermodynamic model capable of simulating monthly mean sea level pressure for both climatology and variations with time scales ranging from months to years. In section 2 we examine momentum balance in the boundary (or surface) layer using observations. Use of anisotropic, latitude-dependent Rayleigh friction coefficients is shown to significantly reduce errors in simulation of observed monthly mean surface winds, given the observed monthly mean pressure field. Section 3 discusses the relationships between SST and SLP fields. We will demonstrate that the spatial and temporal variation of the vertically averaged lapse rate is critical for predicting an accurate surface pressure field. A parameterization of the spatiotemporal variation of the averaged lapse rate in terms of SST is proposed. The analyses in sections 2 and 3 lead to the formulation of a simple tropical atmospheric model relevant to the simulation of monthly mean surface winds and precipitation. Section 4 shows the model's performance in simulation of annual cycles as well as monthly mean anomalies associated with the Southern Oscillation.

2. Linear dynamics of the surface momentum balance

Let us start from momentum equations near the surface:

$$\partial u/\partial t + u\partial u/\partial x + v\partial u/\partial y - fv = -\partial\phi/\partial x - Eu, \quad (2.1a)$$

$$\partial u/\partial t + u\partial v/\partial x + v\partial v/\partial y + fu = -\partial\phi/\partial y - Ev, \quad (2.1b)$$

where E stands for a constant Rayleigh friction coefficient. On synoptic time scale, the advection of momentum is an essential ingredient near the equator in the surface momentum balance because of the small Coriolis force (e.g., Mahrt 1972; Young 1987). Assume $u = \bar{u} + u'$ and $v = \bar{v} + v'$, where overbars denote monthly mean and primes denote departures from the monthly mean. The monthly mean momentum equations can then be written

$$\partial\bar{u}/\partial t = -(\bar{u}\partial\bar{u}/\partial x + \bar{v}\partial\bar{u}/\partial y) + f\bar{v} - \partial\bar{\phi}/\partial x - (E\bar{u} + \overline{u'\partial u'/\partial x + v'\partial u'/\partial y}), \quad (2.2a)$$

$$\partial\bar{u}/\partial t = -(\bar{u}\partial\bar{v}/\partial x + \bar{v}\partial\bar{v}/\partial y) - f\bar{u} - \partial\bar{\phi}/\partial y - (E\bar{v} + \overline{u'\partial v'/\partial x + v'\partial v'/\partial y}), \quad (2.2b)$$

where the term on the left-hand side is a local acceleration of the monthly mean wind, which vanishes for the steady-state solution; the first term on the rhs represents an inertial force associated with mean momentum advection; the second and third terms on the rhs denote the Coriolis force and pressure gradient force, respectively; and the last term on the rhs is a residual force, which includes both Rayleigh friction and nonlinear transient effect.

By diagnosing boundary-layer momentum balance using observed climatological monthly mean SLP and surface wind fields, we try to estimate the relative importance of the forces in (2.2a,b). The data are derived from COADS (Comprehensive Ocean–Atmosphere Data Set) for the period of 1900–79 (Sadler et al. 1987). Resolution is 2 degrees longitude by 2 degrees latitude.

Figure 1 shows the geographic distribution of the four terms (pressure gradient force, Coriolis force, inertial force, and residual force). There are several noticeable features.

1) The pressure gradient force and Coriolis force tend to have opposite signs and comparable magnitudes except within 3°–5° latitude of the equator. Both fields have a dominant meridional component.

2) The inertial force (or mean momentum advection) can be neglected compared to the pressure gradient and Coriolis forces. Along the equator, the zonal averaged magnitudes of pressure gradient and inertial forces are 2.3×10^{-5} m s^{-2} and 0.3×10^{-5} m s^{-2}, respectively, in the zonal direction, and 3.9×10^{-5} m s^{-2} and 0.2×10^{-5} m s^{-2}, respectively, in the meridional direction. This is consistent with the conclusions of the previous studies (e.g., Zebiak 1990).

3) The residual term, which consists of frictional and nonlinear transient effects, is comparable with the

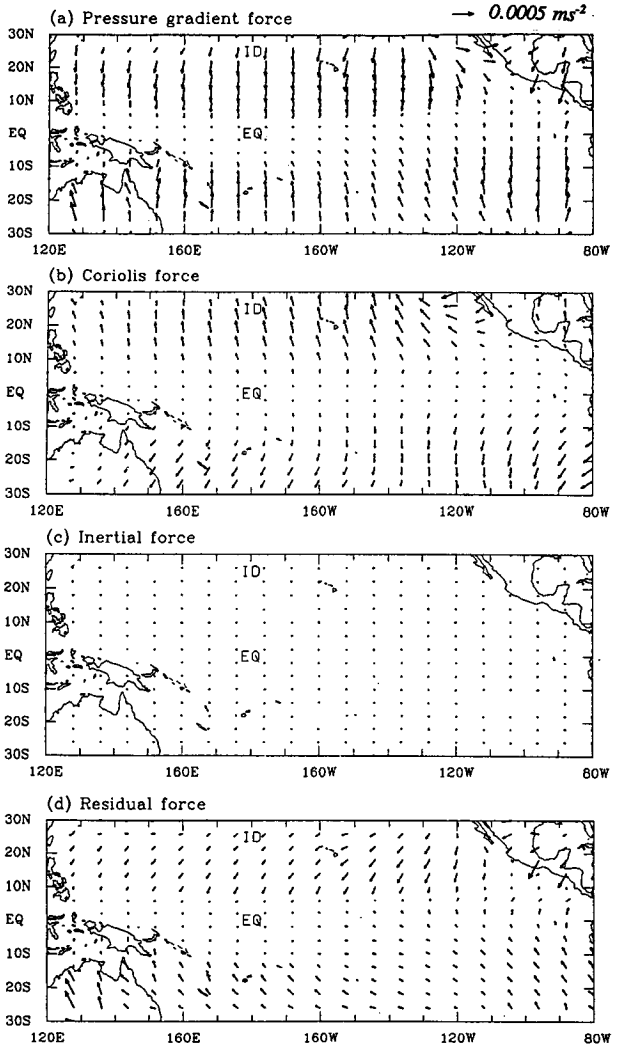

FIG. 1. The (a) pressure gradient force, (b) Coriolis force, (c) inertial force, and (d) residual force computed from climatological annual mean sea level pressure and surface winds derived from COADS by Sadler et al. (1987).

pressure gradient and Coriolis forces. The direction of the residual force is generally in good agreement with the observed surface wind field, particularly in the trade wind regions. This agreement suggests that the combined frictional and transient effects may be parameterized by, to the first approximation, a form of Rayleigh friction.

Thus, the linear boundary-layer momentum equations for monthly mean steady-state motion on the equatorial β plane can be written as

$$E_1 u - \beta y v = -\partial\phi/\partial x, \quad (2.3a)$$

$$E_2 v + \beta y u = -\partial\phi/\partial y, \quad (2.3b)$$

where u, v, and ϕ denote monthly mean boundary-layer (or 1000 mb) zonal and meridional wind components and geopotential height, respectively. Here E_1 and E_2 are parameterized zonal and meridional Rayleigh friction coefficients, and

$$E_1 u = Eu + \overline{u'\partial u'/\partial x + v'\partial u'/\partial y} \quad (2.4a)$$

$$E_2 v = Ev + \overline{u'\partial v'/\partial x + v'\partial v'/\partial y}. \quad (2.4b)$$

Equations (2.4a,b) indicate that a variable Rayleigh friction coefficient is a result of parameterization of transient Reynolds stresses, which may change with space and time.

In previous simple or intermediate models a common practice was to assume a constant Rayleigh friction coefficient of 10^{-5} s^{-1} in both zonal and meridional momentum equations (Zebiak 1982; Davey and Gill 1987; Murphree and Van den Dool 1988; and others). The corresponding damping time scale is about one day. Using this constant Rayleigh friction coefficient, we have computed the surface winds from the annual mean SLP field based on the three-force balance model with proper smoothing. The difference between simulated and observed winds is shown in Fig. 2. In general, the simulated trade wind between 10°N to 20°N is too strong and too zonal, whereas the equatorial easterlies are relatively weak with a maximum error of 1–2 m s^{-1} in the eastern equatorial Pacific. The largest discrepancy of the zonal component (greater than 3 m s^{-1}) occurs along the coast of Mexico and Central America. The most serious error is the simulated meridional wind component in the equatorial eastern Pacific where the error is up to 7 m s^{-1}. The large error in meridional wind severely affects convergence in the ITCZ. Further sensitivity tests indicate that, whereas decreasing the friction coefficient can increase the equatorial easter-

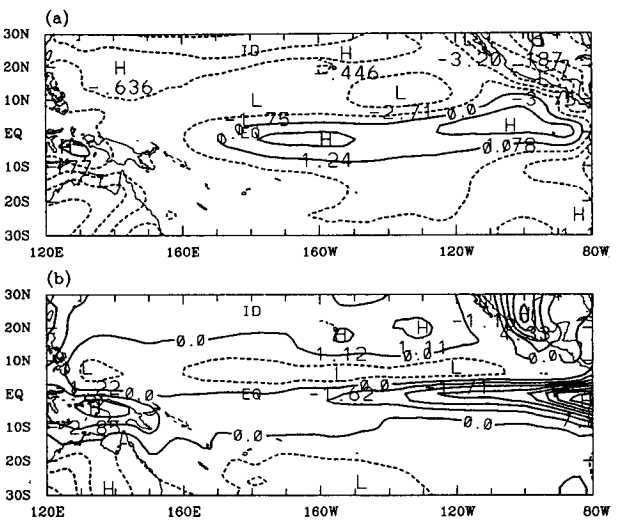

FIG. 2. The difference between simulated and observed annual mean surface (a) zonal and (b) meridional winds (in units m s^{-1}). The simulation uses a linear three-force balance model (2.3) with a constant Rayleigh friction coefficient of 10^{-5} s^{-1}.

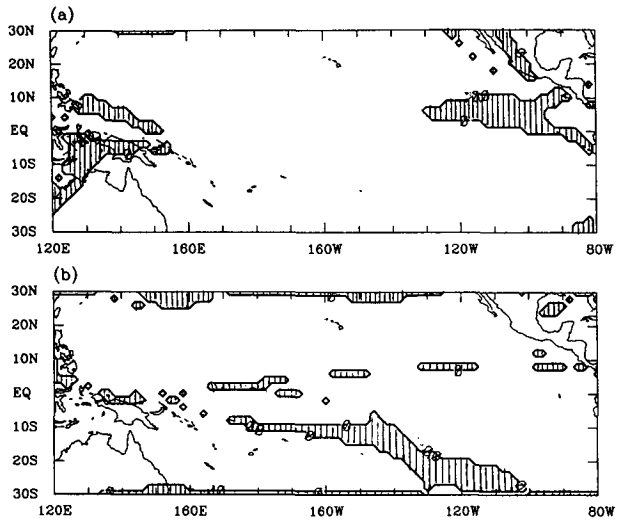

FIG. 3. Geographic distribution of the regions (represented by shading areas) where opposite signs exist between the residual force and surface wind in (a) zonal and (b) meridional directions.

lies, the trade winds become more zonal and the cross-equator meridional wind unrealistically large. As a result, the corresponding convergence field near the equator becomes worse. With increasing friction coefficients the simulated trade winds are closer to the observed, but the equatorial easterlies become too weak. Similar flaws exist when climatological monthly mean data were used.

The results suggest that if the linear momentum balance equation is used to model monthly mean surface winds, the Rayleigh friction coefficients in zonal and meridional directions, which parameterize the frictional and transient effects, should not be treated as a constant; rather, they must vary with space and time. The friction coefficients might be larger over land than over the ocean. Their spatial and temporal variations can also be due to the effects of transient disturbances on various time scales.

Using observed climatological annual mean pressure and wind field, the parameterized Rayleigh friction terms can be evaluated by the linear momentum balance. The results indicate that there are areas where the residual (or parameterized Rayleigh friction) terms have opposite signs with corresponding zonal or meridional wind components (Figs. 3a,b). In those regions, a negative Rayleigh friction is implied if the linear balance model (2.3) is used. The negative friction areas indicate important dynamical regions in the tropical Pacific boundary layer where the traditional view of the three-force balance in the tropical boundary layer breaks down. If the observations used for computation are precise, the negative friction implies that nonlinear transient effects play a decisive role in maintaining momentum balance. For the u-momentum balance, such negative friction regions are located primarily in the equatorial western Pacific monsoon region and the eastern North Pacific summer monsoon domain. The prominent eastern North Pacific summer monsoon is characterized by the establishment of southwesterly flows south of the monsoon trough (Murakami et al. 1992). The strong annual cycle as well as high-frequency transient activity could effectively modify annual mean flows. The transient effects in the eastern North Pacific can be thought of as westerly momentum sources for the annual mean field. For the v-momentum balance, negative friction regions are located east of the South Pacific convergence zone (SPCZ) and extratropical regions. It is important to note that in those regions, the linear three-force momentum balance fails to reproduce tropical low-level (surface) flows.

Figure 4 shows horizontal distributions of the Rayleigh friction coefficients E_1 and E_2 calculated using observed annual mean SLP and surface winds and modified linear balance momentum equations (2.3a,b). The SLP field has been transferred to geopotential height at a constant pressure (1000 mb) level according to the hydrostatic relationship. To avoid negative and extremely large positive values, the regions where calculated friction coefficients, E_1 and E_2, are greater than $3 \times 10^{-5}\ s^{-1}$ or smaller than $3 \times 10^{-6}\ s^{-1}$ were avoided and interpolation was used to obtain modified values. The friction coefficients in the regions where u and v are less than 0.5 m s^{-1} were also interpolated. It is observed that the zonal friction coefficient E_1 (Fig. 4a) is significantly smaller than the meridional friction coefficient E_2 (Fig. 4b), particularly in the equatorial region where E_2 is up to 3–5 times as large as E_1. The friction coefficients tend to increase with latitude and have larger values over land than over the ocean.

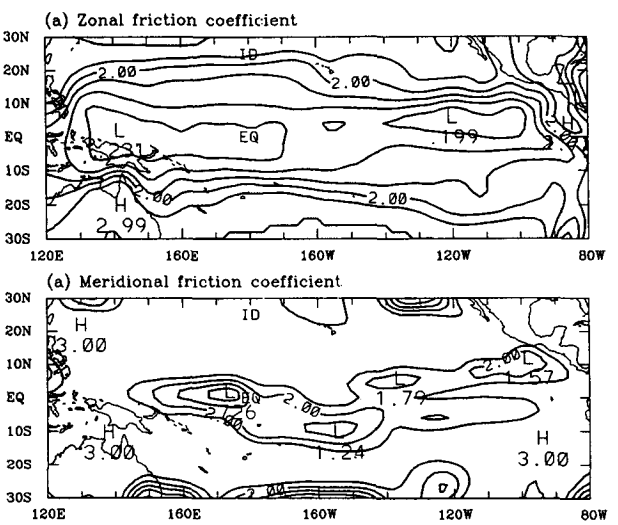

FIG. 4. Diagnosed annual mean (a) zonal and (b) meridional friction coefficients (in units $10^{-5}\ s^{-1}$) based on observation.

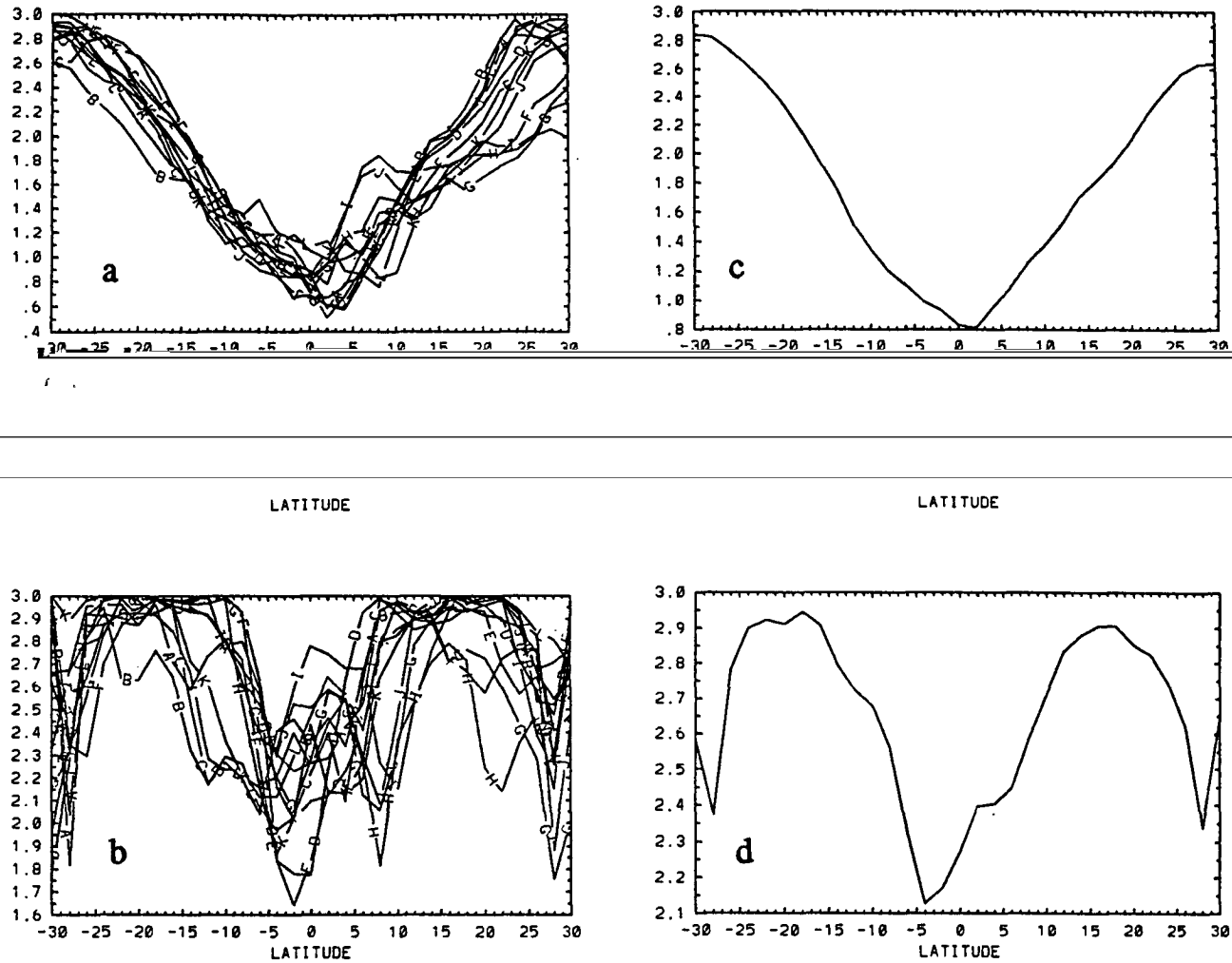

FIG. 5. The meridional distribution of zonal-averaged (a) zonal and (b) meridional friction coefficients for January (line A) through December (line L), and 12-month-mean (c) zonal and (d) meridional (in units 10^{-5} s^{-1}) coefficients.

An important feature in Fig. 4 is that the meridional variations of both E_1 and E_2 are much larger than the corresponding zonal variations. Figures 5a and 5b illustrate zonal-averaged friction coefficients E_1 and E_2 as functions of latitude computed by using climatological monthly mean SLP and surface winds from January through December for the domain between 120°E and 80°W. The 12-month mean E_1 and E_2 are shown in Figs. 5c and 5d. We note that both E_1 and E_2 exhibit a consistent latitudinal dependence for all 12 months. Therefore, the 12-month mean latitude-dependent friction coefficients can be used as a time-dependent quantity in reproducing the annual cycle. Generally, the zonal friction coefficient is smallest at the equator and increases with latitude. The meridional friction coefficient is smallest between the equator and 5°S and largest around 20°N or 20°S. Both zonal and meridional friction coefficients are approximately symmetric with respect to the equator. Near the equator between 10°S and 10°N the annual mean zonal-averaged E_2 is 2–2.5 times as large as E_1. This result agrees with Deser's (1993) recent study.

Significantly improved simulation of the surface winds can be obtained by use of anisotropic, latitude-varying friction coefficients in the linear horizontal momentum equations. Figures 6a and 6b show the difference between the simulated and observed zonal and meridional winds using latitude-dependent friction coefficients shown in Figs. 5c and 5d and observed annual mean SLP. The friction over land is set five times greater than over the ocean. The same smoothing used in Fig. 2 was applied. The difference between the simulation and observation is, in most regions, less than 1 m s^{-1} in both zonal and meridional components. Thus, the magnitude and location of both zonal and meridional winds are well simulated. For instance, the simulated trade winds and equatorial easterlies are both close to the observed. Convergence along ITCZ is well reproduced.

We conclude that the use of anisotropic, latitude-dependent friction coefficients is critical for successfully simulating surface (or low-level) wind field in a simple three-force balance boundary-layer model.

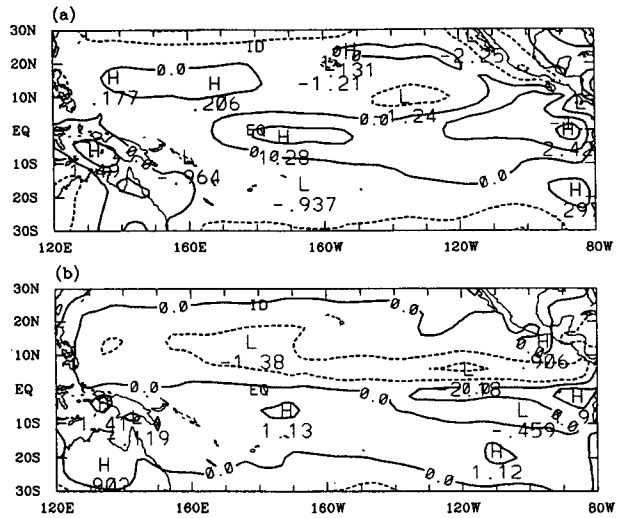

FIG. 6. As in Fig. 2 except with latitude and direction-dependent Rayleigh friction coefficients.

3. A simple model of the monthly mean sea level pressure

Lindzen and Nigam (1987) first emphasized the importance of the SST gradient in forcing boundary-layer flows. Their boundary-layer model involves a pressure gradient that is induced by SST gradients via hydrostatic equilibrium, assuming that the boundary-layer air is well mixed by surface buoyancy fluxes. A major flaw of the model is the treatment of the so-called back pressure effect. The pressure change at the top of the boundary layer was assumed to be caused by adiabatic cooling associated with the boundary-layer mass convergence (Wang and Li 1993). The effects of the free atmospheric heating and motion were completely disregarded. On the other hand, Davey and Gill's (1987) model considered the effect of SST on midtropospheric heating via longwave radiational processes, assuming that the midtropospheric temperature tends to relax, within a certain Newtonian cooling time scale, toward a hypothetical equilibrium state that is determined by SST.

We now extend and combine those ideas to propose a quasi-equilibrium model for monthly mean sea level pressure. Consider a moist hydrostatic equilibrium troposphere with a vertically averaged lapse rate γ, that is, $T_v(z) = T_s - \gamma z$, where T_v is virtual temperature and T_s is surface virtual temperature, which for simplicity is assumed to be equal to SST. The top of the troposphere is assumed undisturbed with constant pressure (p_u) and height H. This assumption is approximately valid for the tropical troposphere between 20°N and 20°S. For a moist hydrostatic atmosphere,

$$\partial p/\partial z = -gp/RT_v, \tag{3.1}$$

where p, g, and R represent the pressure, gravity, and gas constant for dry air. Integrating (3.1) vertically from surface $z = 0$ to the tropopause $z = H$ yields

$$\ln(P_s/P_u) = (g/R\gamma)\ln[T_s/(T_s - \gamma H)], \tag{3.2}$$

where P_s stands for SLP. For a constant mean lapse rate (6°C/km) and a tropopause at 100 mb, the height (H) of the tropopause is 16.8 km as determined by (3.2) if domain-averaged (30°S–30°N, 120°E–80°W) annual mean SST and SLP are used as reference temperature and pressure. The calculated tropopause height is close to the observed value in the tropics.

Generally speaking, the model lapse rate γ should change with time and space. By applying climatological monthly mean SST and SLP data in Eq. (3.2), we can compute mean vertically averaged lapse rate (hereafter referred to as model lapse rate). Figure 7a shows geographic distribution of the model lapse rate for January, April, July, and October. Note that the lapse rates display a reasonable range of variation from 6.4°C/km to 5.4°C/km. To compare them with observations, we have computed the vertically averaged lapse rate fields for the corresponding months using climatological monthly mean 200- and 850-mb geopotential height fields derived from the European Centre for Medium-Range Weather Forecasts by the following formula:

$$\begin{aligned}\phi_2 - \phi_1 = {} & -RT_s\ln(p_2/p_1) + R\gamma[\phi_2\ln(p_2) \\ & - \phi_1\ln(p_1)]/g - R\{\gamma(\phi_2 - \phi_1) \\ & \times [\ln(P_s)/g - \ln(T_s)/(R\gamma)] \\ & - g/(R\gamma)[(T_s - \gamma\phi_2/g)\ln(T_s - \gamma\phi_2/g) \\ & - (T_s - \gamma\phi_1/g)\ln(T_s - \gamma\phi_1/g) \\ & + \gamma(\phi_2 - \phi_1)/g]\},\end{aligned} \tag{3.3}$$

where subscripts 1 and 2 represent, respectively, 200 mb and 850 mb, and all variables have their conventional meaning. Equation (3.3) is derived from the vertically integrated hydrostatic equation with an application of the equation of state for an ideal gas. The results, as shown in Fig. 7b, are referred to as the observed field. The gross resemblance between the model lapse rate and observed lapse rate (within 20°N and 20°S) lends support to the validity of the simple model of monthly mean SLP, (3.2).

Both Figs. 7a and 7b show that larger lapse rates occur in higher SST regions. The annual variation of the lapse rate exhibits a systematic meridional migration in the western Pacific, following closely the annual variation of SST. In fact, there is a high correlation between SST and the model lapse rate. The linear correlation coefficient calculated for the entire tropical Pacific domain (30°S–30°N, 120°E–80°W) and for all 12 months (sample size: 30132), is 0.99. The linear regression equation for lapse rate can be expressed as

$$\gamma_{\text{regression}}(°\text{C/km}) = 10^{-3}[0.0956T_s(°\text{C}) + 3.54]. \tag{3.4}$$

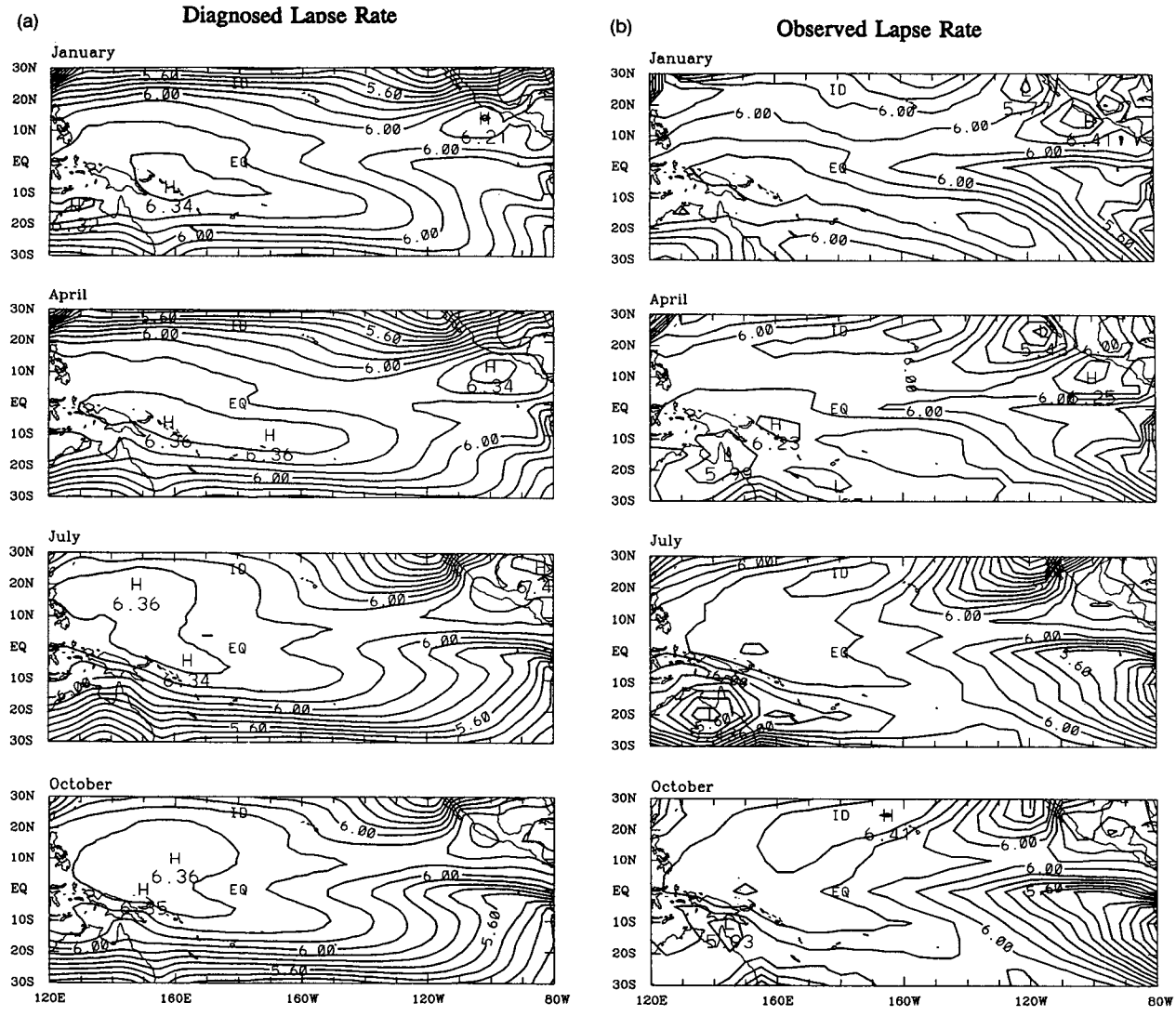

FIG. 7. (a) The model-diagnosed January, April, July, and October lapse rate (in units °C/km) distribution calculated from Eq. (3.2) by using observed climatological monthly mean SST and SLP (COADS) data. (b) As in (a) except that the lapse rate is calculated from Eq. (3.3) using ECMWF analyzed climatological geopotential height at 200 and 850 mb.

Using this empirical formula, an excellent estimate of lapse rate can be made from SST. Thus, for given monthly mean SST, monthly mean sea level pressure can be determined from (3.2) with $\gamma = \gamma_{\text{regression}}$.

It is important to point out that the lapse rate estimated by (3.4) has a systematic bias compared to the model lapse rate. The 12-month-averaged bias (estimated minus model lapse rate) is shown in Fig. 8. The amplitude of the bias is about 0.05°C/km. We note that there are two negative centers in the subtropical high regions, indicating that the empirical equation (3.4) underestimates the model lapse rate in these regions. This implies that in the subtropical high regions the use of (3.4) would overestimate the tropospheric mean temperature, resulting a lower than observed SLP. On the other hand, two areas of major positive bias are found in the cold SST tongue regions along coasts of South America and Mexico. Over those regions the use of (3.4) tends to underestimate the mean tropospheric temperature and results in a higher than observed SLP. It is worth noting that the annual variation of the bias is negligible, that is, the bias is nearly season independent and is primarily a function of geographic locations. It can be included for a steady-state climate model by

$$\gamma = \gamma_{\text{regression}} + \gamma_{\text{bias}}. \tag{3.5}$$

The premise involved here is that the principal part of the vertical mean lapse rate is determined by SST (via $\gamma_{\text{regression}}$ term), whereas the effects of other unresolved

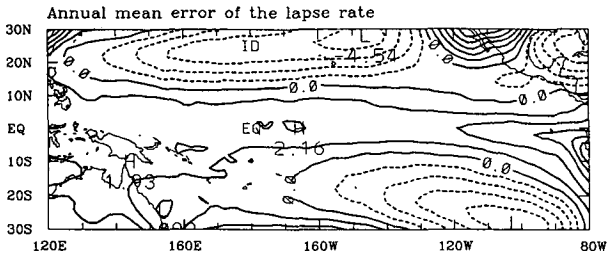

FIG. 8. The 12-month-mean difference between empirical lapse rate calculated from Eq. (3.4) and diagnosed lapse rate calculated from Eq. (3.2). The contour interval is 0.01°C/km.

free atmospheric processes, especially the transient and radiational heating processes, are parameterized by γ_{bias} term. The latter affects the nature of mean climate systems.

The time-independent bias is empirically determined from climatological data (Fig. 8). Inclusion of this empirical correction in estimation of γ improves the simulation of the locations of subtropical highs in both hemispheres, reproducing a more realistic annual cycle of SLP from a given SST field.

4. The simple climate model and its performance

a. The model

Based on the diagnostic analysis and formulations in the previous two sections, a simple model for tropical SLP, surface winds, and precipitation is proposed. First, the SLP can be predicted from the underlying SST field using the vertically integrated hydrostatic equation and equation of state: Eq. (3.2) along with (3.4) and (3.5). The modification of the estimated lapse rate (3.5) is necessary and represents parameterized dynamic and radiational feedbacks of the tropospheric motion to changes in SLP. Once SLP is obtained, surface winds can be readily computed using the linear three-force balance momentum equation (2.3) with anisotropic, latitude-dependent Rayleigh friction coefficients E_1 and E_2 (Figs. 5c,d). Precipitation rate can then be determined by the sum of the boundary-layer moisture convergence and local evaporation,

$$P_r = \delta b\{-\rho_s \Delta z \nabla\cdot(q_a \mathbf{V}_B) + \rho_s C_D |\mathbf{V}_B|(q_s - q_a)\}. \tag{4.1}$$

Here we have assumed that moisture convergence takes place only in the well-mixed boundary layer. For a detailed derivation refer to WL. In (4.1) C_D is the drag coefficient (0.0015); ρ_s is surface air density (1.2 kg m^{-3}); b is a precipitation efficiency coefficient (0.75), which denotes the ratio of the precipitation to total moisture convergence plus evaporation, following Kuo (1974); Δz is the depth of the boundary layer (1500 m); $\mathbf{V}_B$ represents time-mean surface wind speed (to consider transient and turbulent effects on local evaporation, when $\mathbf{V}_B$ is smaller than 4 m s^{-1} a constant value of 4 m s^{-1} is used); δ is a switch-on coefficient for SST-dependent nonlinear heating as proposed by Wang and Li (1993); q_s is the specific humidity at the sea surface, which is a function of SST and SLP; and q_a is the surface air specific humidity, which can be empirically determined from SST. The linear correlation coefficient between SST and q_a computed for all 12 months and entire model domain exceeds 0.99. The linear regression equation between SST and q_a can be written as

$$q_a = 10^{-3}[0.972T_s(°\text{C}) - 8.92]. \tag{4.2}$$

The surface air specific humidities used to obtain the regression equation (4.2) are from Esbensen and Kushnir (1982) with the resolution of 5 degrees longitude by 4 degrees latitude and total sample size of 5760.

b. Modeling of the annual cycles

Annual variations of tropical Pacific SLP, surface winds, and precipitation are simulated using the present model forced by climatological monthly mean SST. The domain of the forcing spans 30°S to 30°N, 120°E to 80°W with a resolution of 2 degrees longitude by 2 degrees latitude. A nine-point smoothing method with weights of 4, 2, and 1 is applied to the resultant surface wind fields. Figure 9a presents the simulated climatological monthly mean SLP and surface winds. For comparison, the observed SLP and surface winds (Sadler et al. 1987) for the corresponding months are illustrated in Fig. 9b. The pressure difference between the simulated and observed fields is within 1–2 mb in most regions. Many fundamental features of the annual cycle of SLP and surface winds are reasonably well reproduced. For instance, the position and intensity of the subtropical highs and trade winds in both hemispheres are well simulated. In the western Pacific, there is an obvious annual variation of monsoon circulation with reversed cross-equatorial flow from winter to summer hemispheres. In the eastern Pacific, the cross-equatorial southerly component reaches a maximum in July and October when the ITCZ or eastern North Pacific monsoon trough reaches its northernmost position. The southwesterly flow is also found north of the equator during the eastern North Pacific summer monsoon. The trade wind convergence zone (the ITCZ in the central Pacific) is found close to the equator in April and at its northernmost location in October. The South Pacific convergence zone (SPCZ) is strongest in January but nearly disappears in July.

The annual cycle of precipitation pattern is consistent with surface wind and pressure variations. Figure 10a illustrates the mean precipitation rate in January, April, July, and October. As an indirect comparison, observed climatological monthly highly reflective cloud (HRC) data derived by Garcia (1985) are dis-

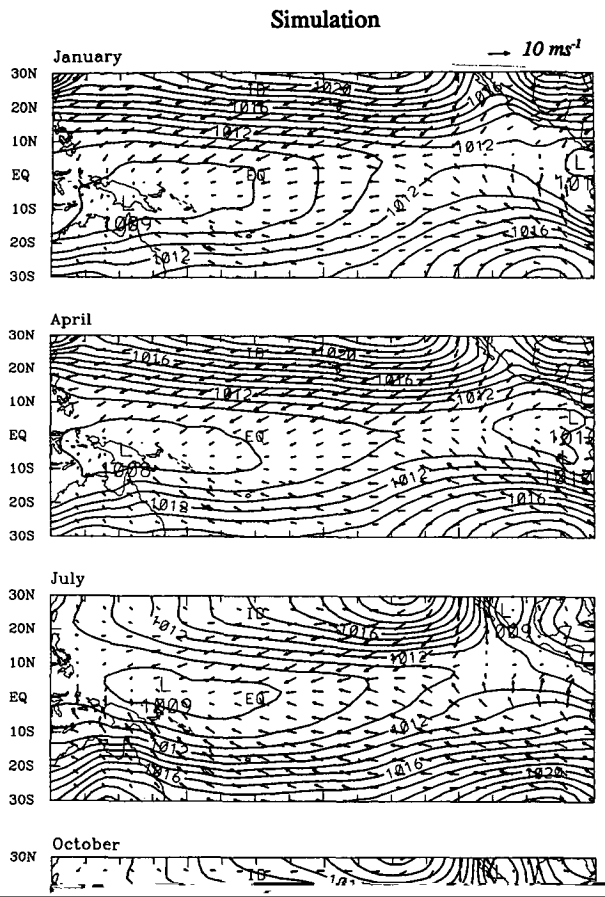

precipitation shows double ITCZs in April, which are observed on satellite cloud pictures. The simulated precipitation rate along the ITCZ in the central Pacific shows a maximum in October and a minimum in January, which is also in agreement with observations (Wang 1993). The major discrepancy of the simulated precipitation field lies in its strength in the SPCZ region during the northern winter where the observed highly reflective cloud shows the maximum value. Because the SPCZ is a deep convergence zone in the lower troposphere, whereas the model precipitation only takes boundary-layer moisture convergence into account, this discrepancy is expected. It may be improved by assuming a space-varying depth of boundary layer.

c. *Modeling of anomalies associated with the Southern Oscillation*

Figure 11 shows monthly mean SST anomalies for January 1983 and December 1988. The former is representative of the mature phase of the 1982–83 Pacific warm event, whereas the latter is representative of the mature phase of the 1988–89 cold event. The monthly mean SST fields for the two selected months were used to force the conceptual model. The model climatology was then subtracted from the resultant total circulation field so that the simulated monthly mean anomalies can be conveniently compared with their observed counterparts.

The simulated surface wind and precipitation anom-

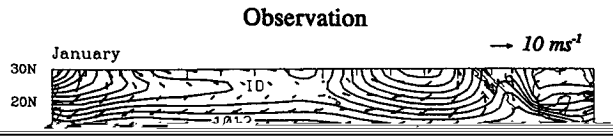

Pacific, the observed SLP anomaly field shows two minimum pressure centers (with respective maximum anomalies of 2.3 and 1.6 mb), corresponding to the 1982–83 and 1986–87 warm events. The simulated

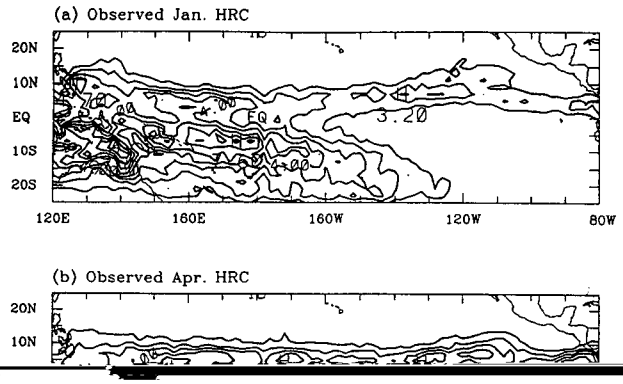

we found that it is extremely difficult to accurately predict sea level pressure (SLP) even using observed surface wind and divergence fields, suggesting that the physics included in these model is insufficient for this purpose. An example is the failure of reproducing the zonal phase shift between the cold SST tongues and the subtropical highs so that the simulated easterly trades equatorward of the subtropical highs and the alongshore meridional winds near Mexico and South America are weaker than the observed. The exact physical mechanisms causing the phase shift remain to be investigated. We speculate that the effects of transient

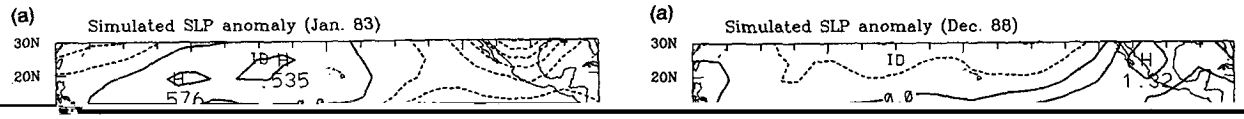
(a)
Simulated SLP anomaly (Jan. 83)
30N
20N
1D
535
576
(a)
Simulated SLP anomaly (Dec. 88)
30N
20N
1D
SH
1.32
0.0

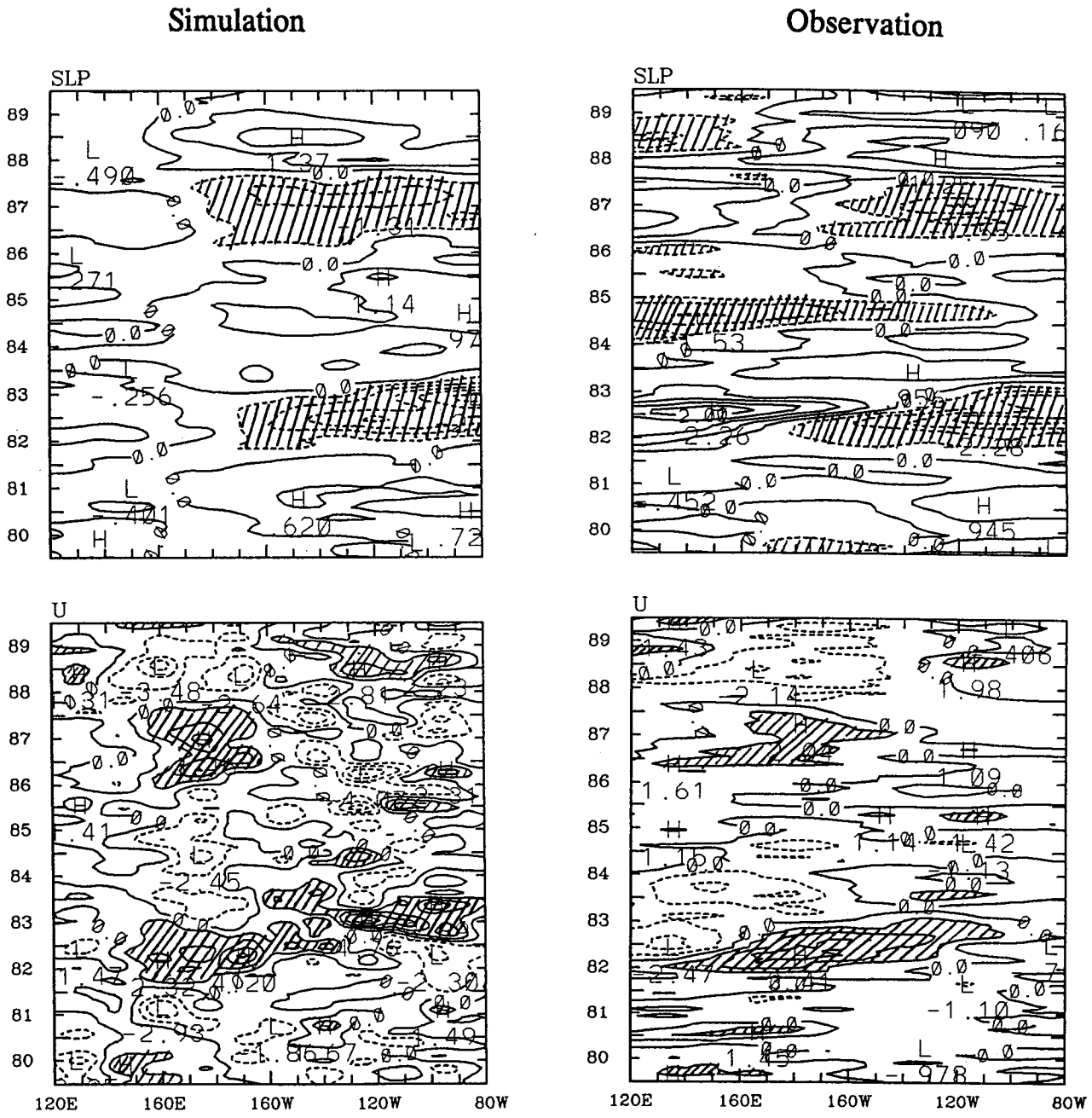

FIG. 14. The model-simulated (left panel) and observed (right panel) SLP and surface zonal wind anomalies along the equator for 10-year period from January 1980 to December 1989. The areas of lower than −0.5 mb for SLP anomaly or greater than 1 m s^{-1} for zonal wind anomaly are shaded.

rate correction parameterizes the effects of transient and radiational heat processes.

The analysis of monthly mean surface momentum balance indicates that the monthly mean inertial force is not important, but the parameterization of the transient (nonlinear) eddy effects on the monthly mean surface momentum balance is necessary. To the lowest order of approximation, the eddy effects can be taken into account by an empirical Rayleigh friction form that changes with latitude and direction. The use of latitude- and direction-dependent Rayleigh friction coefficients is critical for the linear momentum balance model to predict realistic monthly mean surface winds from monthly mean SLP.

In spite of its simplicity, the present model is able to reproduce a reasonably realistic annual cycle and interannual variability of the tropical surface winds, SLP, and precipitation at extremely low computational costs. The success of the proposed model suggests that, to the lowest order approximation, the monthly mean SLP can be estimated by a moist hydrostatic *equilibrium* atmosphere whose temperature at the surface and vertical mean lapse rate are determined by the underlying SST. We speculate that the dynamic feedback of vertical motion (or low-level divergence) on surface pressure is of secondary importance, but necessary for an *accurate* prediction of surface pressure. That, however, requires a more complicated treatment than what is described by the existing simple or intermediate model physics. The present model crucially parameterizes tropospheric dynamics and other missing physics by an empirical SST–mean lapse rate relationship. Within this model framework a spatial and temporal varying static stability is critical for the thermodynamic balance in the tropical troposphere. The proposed model for monthly mean SLP provides a simplified view of how the complex variation of monthly mean SLP in the tropics is controlled by SST. The model is based on an thermodynamic framework of hydrostatic equilibrium tropical atmosphere with a crude parameterization of the effects of dynamic processes on an empirical ground. We must admit that there is little physical basis for the proposed parameterization, although speculations have been offered to motivate the parameterization. Further studies are needed to put the parameterization on a firm physical basis.

In a coupled ocean–atmosphere model for prediction of El Niño, the ocean model requires its atmospheric counterpart to provide as accurate surface winds and precipitation/cloudiness as possible. It would be interesting to see how the coupled system behaves when the present model is coupled with an ocean GCM or ocean models with intermediate complexity such as Zebiak and Cane (1987) and Anderson and McCreary (1985).

Acknowledgments. This work is supported by Tropical Ocean–Global Atmosphere Program of NOAA under Grant NA90RAH00074 through the Joint Institute for Marine and Atmospheric Research. We appreciate the comments provided by Dr. R. Seager and an anonymous reviewer. Thanks to Dr. T. Schroeder for his editorial assistance.

REFERENCES

Anderson, D. L. T., and J. P. McCreary, 1985: Slowly propagating disturbances in a coupled ocean–atmosphere model. *J. Atmos. Sci.*, **42,** 615–629.

Davey, M. K., and A. E. Gill, 1987: Experiments on tropical circulation with a simple moist model. *Quart. J. Roy. Meteor. Soc.*, **113,** 1237–1269.

Deser, C., 1993: Diagnosis of the surface momentum balance over the tropical Pacific Ocean. *J. Climate,* **6,** 64–74.

Esbensen, S. K., and V. Kushnir, 1982: The heat budget of the global ocean: An atlas based on estimates from marine surface observations. Rep. 29, Clim. Res. Inst., Oreg. State Univ., Corvallis, OR, 27 pp.

Garcia, O., 1985: Atlas of highly reflective clouds for the global tropics: 1971–1973. U.S. Department of Commerce, NOAA, Environmental Research Lab., Boulder, CO.

Gill, A. E., 1980: Some simple solutions for heat-induced tropical circulation. *Quart. J. Roy. Meteor. Soc.*, **106,** 447–462.

Kuo, H.-L., 1974: Further studies of the parameterization of the influence of cumulus convection on large-scale flow. *J. Atmos. Sci.*, **31,** 1231–1240.

Lindzen, R. S., and S. Nigam, 1987: On the role of sea surface temperature gradients in forcing low-level winds and convergence in the tropics. *J. Atmos. Sci.*, **45,** 2440–2458.

Mahrt, L. J., 1972: A numerical study of the influence of advective accelerations in an idealized, low latitude, boundary layer. *J. Atmos. Sci.*, **29,** 1477–1484.

Murakami, T., B. Wang, and S. W. Lyons, 1992: Summer monsoons over the Bay of Bengal and the eastern North Pacific. *J. Meteor. Soc. Japan,* **70,** 191–210.

Murphree, T., and H. van den Dool, 1988: Calculating winds from time mean sea level pressure fields. *J. Atmos. Sci.*, **45,** 3269–3281.

Sadler, J. C., M. A. Lander, A. M. Hori, and L. K. Oda, 1987: *Tropical Marine Climatic Atlas.* Vol. 2, *Pacific Ocean.* Report UHMET 87-02, Department of Meteorology, University of Hawaii, Honolulu, Hawaii, 27 pp.

Seager, R., 1991: A simple model of the climatology and variability of the low-level wind field in the tropics. *J. Climate,* **4,** 164–179.

Taylor, R. C., 1973: *An Atlas of Pacific Island Rainfall.* Hawaii Inst. Geophys. Data Rep., HIG-73-9, 175 pp. [NTIS AD 767073.]

Wang, B., 1994: Climatic regimes of tropical convection and rainfall. *J. Climate,* **7,** in press.

——, and T. Li, 1993: A simple tropical atmospheric model of relevance to short-term climate variations. *J. Atmos. Sci.*, **50,** 260–284.

Webster, P. J., 1981: Mechanisms determining the atmospheric response to sea surface temperature anomalies. *J. Atmos. Sci.*, **38,** 554–571.

Young, J. A., 1987: Physics of monsoons: The current review. *Monsoons,* J. S. Fein and P. L. Stephen, Eds., John Wiley and Sons, 211–243.

Zebiak, S. E., 1982: A simple atmosphere model of relevance to El Niño. *J. Atmos. Sci.*, **39,** 2017–2027.

——, 1986: Atmospheric convergence feedback in a simple model for El Niño. *Mon. Wea. Rev.*, **114,** 1263–1271.

——, 1990: Diagnostic studies of Pacific surface winds. *J. Climate,* **3,** 1016–1031.

——, and M. A. Cane, 1987: A model El Niño–Southern Oscillation. *Mon. Wea. Rev.*, **115,** 2262–2278.